Umbilical Cord Blood-Derived Mesenchymal Cell Fate After Mouse Umbilical Cord Blood Transplantation

Umbilical cord blood (UCB)-derived mesenchymal stem cells (MSCs) not only have the potential to differentiate into multilineage cells, including mesenchymal lineage cells but also can form neurons, skeletal muscle, and myocardium (*1–5*). UCB is also an attractive source of hematopoietic stem cells (HSCs) and has many advantages over bone marrow transplantation, including a larger size of available donor pool, enriched hematopoietic progenitor cells (*6*), low content of mature T cells capable of causing graft-versus-host reactions (*7, 8*), and absence of cytomegalovirus infection (*9*). Accumulating clinical evidence demonstrates that the total number of nucleated cells in a given UCB unit is the single most important parameter for a successful transplantation outcome, with low cell

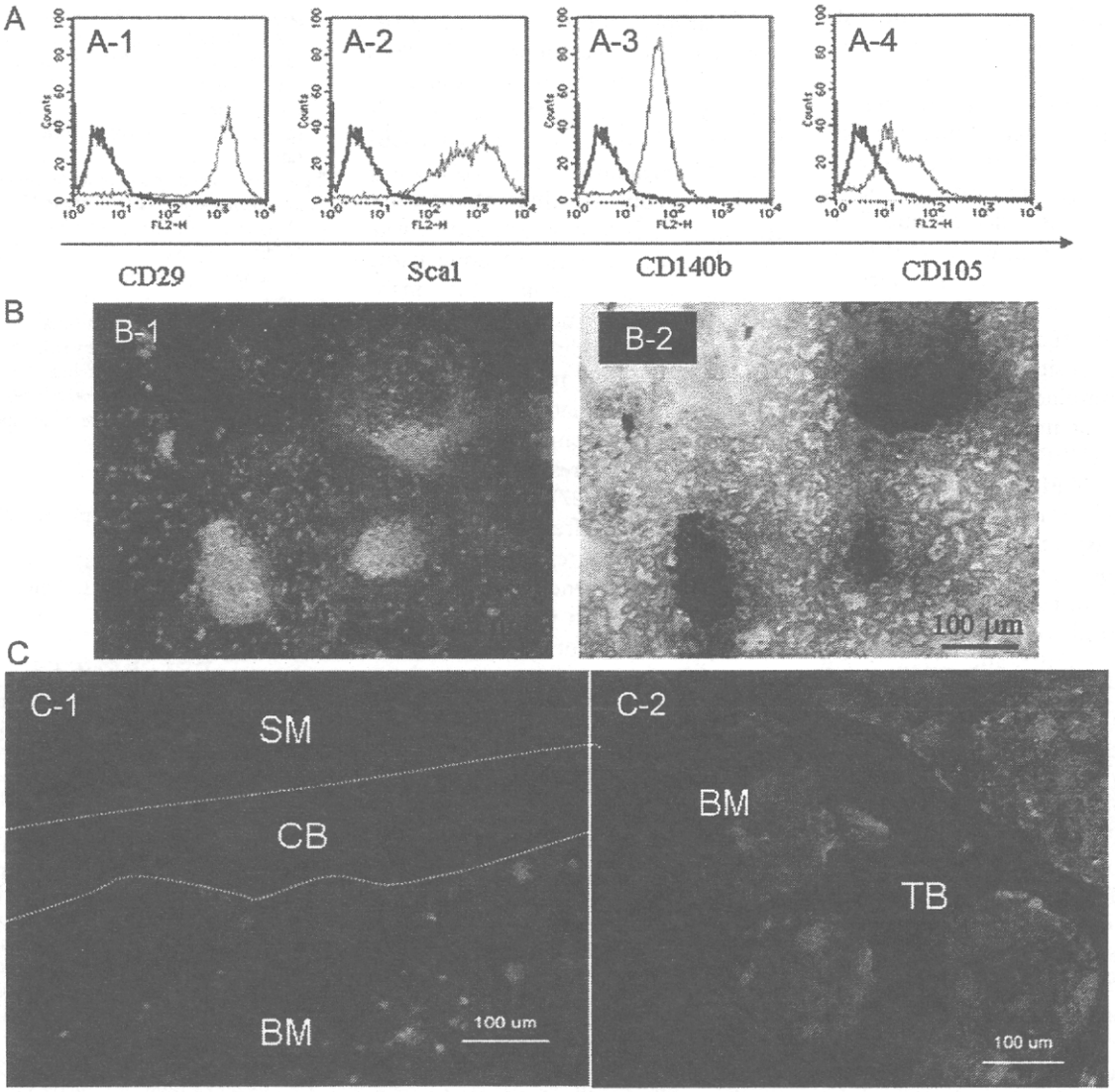

FIGURE 1. Analysis of osteoblastic differentiation potential, mesenchymal stem-cell-related markers, and distribution after umbilical cord blood transplantation. (A) Flow cytometric analysis of adherent cells in the bone marrow of C57BL/6 mice after umbilical cord blood transplantation. A-1: CD29; A-2: Sca-1; A-3: CD140b; and A-4: CD105. *Blue line*: nonstained control and *red line*: stained sample. (B) Osteoblast differentiation potential of GFP-positive adherent cells after in vitro induction. B-1: fluorescence microscopic observation and B-2: phase-contrast microscopic observation after Von Kossa staining. The scale bars represent 100 μm. (C) Distribution of GFP-positive cells in musculoskeletal tissue after umbilical cord blood transplantation. The presence of GFP-positive cells in femoral metaphysis (C-1) and femoral diaphysis (C-2). SM, skeletal muscle; CB, cortical bone; BM, bone marrow; TB, trabecular bone; GFP, green fluorescent protein. The scale bars represent 100 μm.

numbers frequently resulting in delayed or failed engraftment (*10, 11*). Recent studies have also reported that bone marrow MSCs play important roles for hematopoietic reconstitution after HSC transplantation (*12, 13*). Although UCB-derived MSCs may be important for UCB transplantation, the cell fate of UCB-derived mesenchymal cells after UCB transplantation is mostly unknown. In this study, we investigated the fate of mouse UCB-derived mesenchymal cells after transplantation of UCB into mice using a mouse UCB transplantation model (*14, 15*).

All animal experiments were performed in accordance with the Institutional Guidelines for Animal Care established by Kitasato University. UCB cells obtained from green fluorescent protein (GFP)-transgenic mice were intravenously injected into the irradiated C57BL/6 mice (*14, 15*). After 6 months, bone marrow was collected, and GFP-positive adherent cells were stained with MSC-related marker and analyzed by flow cytometry analysis. The in vitro osteoblastic differentiation potential of isolated GFP-positive bone marrow cells was also examined. In addition, the distribution of umbilical cord blood-derived cells (UCBCs) in the bone tissue of recipient C57BL/6 mice was observed by fluorescence microscopy 6 months after the transplantation.

GFP-positive adherent cells were harvested from recipient bone marrow and expressed MSC-related markers CD29, Sca1, CD105, and CD140b (Fig. 1A). After the in vitro induction of osteoblast differentiation, UCB-derived adherent cells were positive for Von Kossa staining (Fig. 1B). Histological analyses confirmed the ubiquitous presence of UCB-GFP cells in the bone marrow and the trabecular and cortical bone surfaces (Fig. 1C).

Erices et al. (*16*) reported that ex vivo-expanded human UCB-derived MSCs engraft bone marrow after xenogeneic transplantation in nonirradiated nude mice. Before this study, it was also demonstrated that phenotypic changes are induced in MSCs (*17, 18*) and that expanded MSCs display poor tissue tropism when transplanted, including a failure to migrate to the bone marrow (*19, 20*). In contrast, primary bone marrow-derived MSCs (BMSCs) display a low, but efficient, seeding of bone marrow on injection into lethally irradiated hosts (*21, 22*). Because these changes affect the fundamental properties of cells, it is difficult to ascertain whether BMSCs retain or lose their original characteristics, including their apparent in vitro multipotency.

In this study, we transplanted mouse UCB-derived cells into irradiated mice without prior ex vivo culture. We found that recipient bone marrow contained UCBC-derived flask-adherent cells that were positive for several MSC-related markers and differentiated into osteoblastic cells after in vitro induction (Fig. 1A, B). These results suggest that UCB-derived mesenchymal cells engraft after transplantation and maintain osteoblastic differentiation potential. MSCs often commit to the osteocyte lineage after local implantation (*23, 24*). Although bone marrow engrafted UCB-derived mesenchymal cells maintained in vitro osteoblastic differentiation potential, UCBC-derived osteocytes were not observed in recipient bone tissue (Fig. 1C), an observation that is consistent with a recent mice bone marrow transplantation study (*22*).

UCB-derived mesenchymal cells maintain differentiation potential in bone marrow and can differentiate into several cell types in response to environmental cues (*25–27*). Several studies have reported that freshly isolated bone marrow cells can replace part of the hosts' normal mesenchymal or stromal cells (*21, 22, 28*). In this study, mouse UCBCs localized not only to the bone marrow but also to the trabecular bone surfaces, indicating that UCBC-derived mesenchymal cells behave as niche cells after bone marrow engraftment, similar to those derived from BMSCs. Therefore, it is considered that the coinjection of UCB-derived mesenchymal cell may improve the efficacy of UCB transplantation.

In conclusion, mouse UCB-derived mesenchymal cells are capable of bone marrow engraftment after transplantation into irradiated mice and maintaining osteoblastic differentiation potential. A portion of these cells localize to trabecular bone surfaces and may behave as niche cells. Therefore, these results suggest that the transplantation of UCB-derived mesenchymal cells without prior ex vivo culture has clinical utility for accelerating hematopoietic reconstitution after HSC transplantation.

Kentaro Uchida[1]
Ken Urabe[1]
Kouji Naruse[1]
Moritoshi Itoman[2]
[1] Department of Orthopedic Surgery
School of Medicine, Kitasato University
Kanagawa, Japan
[2] Director of Kyushu Rosai Hospital
Kokuraminami, Kitakyushu Fukuoka
Japan

This work was supported in part by grants-in-aid from the Ministry of Education, Sports, Culture, Science and Technology of Japan (K.N. and K.U.); by a grant-in-aid from the Ministry of Health, Labor and Welfare for Research on Human Genome, Tissue Engineering and Food Biotechnology (M.I.); and by research grants from the Parents' Association of Kitasato University School of Medicine. Part of this study was supported by grants for scientific research from Research Project No. 2037 and Postgraduate Research Project No. 3094 from the Graduate School of Medical Science, Kitasato University.
The authors declare no conflict of interest.
Address correspondence to: Kentaro Uchida, Ph.D., Department of Orthopedic Surgery, School of Medicine, Kitasato University, 1-15-1 Kitasato, Minamiku, Sagamihara City, Kanagawa 252-0374, Japan.
E-mail: kuchida@med.kitasato-u.ac.jp
K. Uchida participated in the writing of the paper and performed the research; K. Urabe and M. Itoman participated in research design; and K. Naruse participated in the performance of the research.
Received 15 July 2010.
Accepted 9 August 2010.

ISSN 0041-1337/10/9009-1037
DOI: 10.1097/TP.0b013e3181f674f6

REFERENCES

1. Bicknese AR, Goodwin HS, Quinn CO, et al. Human umbilical cord blood cells can be induced to express markers for neurons and glia. *Cell Transplant* 2002; 11: 261.
2. Erices A, Conget P, Minguell JJ. Mesenchymal progenitor cells in human umbilical cord blood. *Br J Haematol* 2000; 109: 235.
3. Goodwin HS, Bicknese AR, Chien SN, et al. Multilineage differentiation activity by cells isolated from umbilical cord blood: Expression of bone, fat, and neural markers. *Biol Blood Marrow Transplant* 2001; 7: 581.
4. Kakinuma S, Tanaka Y, Chinzei R, et al. Human umbilical cord blood as a source of transplantable hepatic progenitor cells. *Stem Cells* 2003; 21: 217.
5. Rosada C, Justesen J, Melsvik D, et al. The human umbilical cord blood: A potential source for osteoblast progenitor cells. *Calcif Tissue Int* 2003; 72: 135.
6. Wang JC, Doedens M, Dick JE. Primitive human hematopoietic cells are enriched in cord blood compared with adult bone marrow or mobilized peripheral blood as measured by the quantitative in vivo SCID-repopulating cell assay. *Blood* 1997; 89: 3919.

7. Bofill M, Akbar AN, Salmon M, et al. Immature CD45RA(low)RO(low) T cells in the human cord blood. I. Antecedents of CD45RA+ unprimed T cells. *J Immunol* 1994; 152: 5613.
8. Madrigal JA, Cohen SB, Gluckman E, et al. Does cord blood transplantation result in lower graft-versus-host disease? It takes more than two to tango. *Hum Immunol* 1997; 56: 1.
9. Kai S. [Complications of cord blood transplantation: Graft failure and infectious disease]. *Rinsho Ketsueki* 2000; 41: 482.
10. Gluckman E, Rocha V, Boyer-Chammard A, et al. Outcome of cord-blood transplantation from related and unrelated donors. Eurocord Transplant Group and the European Blood and Marrow Transplantation Group. *N Engl J Med* 1997; 337: 373.
11. Rubinstein P, Carrier C, Scaradavou A, et al. Outcomes among 562 recipients of placental-blood transplants from unrelated donors. *N Engl J Med* 1998; 339: 1565.
12. Kim DW, Chung YJ, Kim TG, et al. Cotransplantation of third-party mesenchymal stromal cells can alleviate single-donor predominance and increase engraftment from double cord transplantation. *Blood* 2004; 103: 1941.
13. Lee ST, Maeng H, Chwae YJ, et al. Effect of mesenchymal stem cell transplantation on the engraftment of human hematopoietic stem cells and leukemic cells in mice model. *Int J Hematol* 2008; 87: 327.
14. Migishima F, Oikawa A, Kondo S, et al. Full reconstitution of hematopoietic system by murine umbilical cord blood. *Transplantation* 2003; 75: 1820.
15. Oikawa A, Ito K, Seguchi H, et al. Development of immunocompetent lymphocytes in vivo from murine umbilical cord blood cells. *Transplantation* 2007; 84: 23.
16. Erices AA, Allers CI, Conget PA, et al. Human cord blood-derived mesenchymal stem cells home and survive in the marrow of immunodeficient mice after systemic infusion. *Cell Transplant* 2003; 12: 555.
17. Uchida K, Urabe K, Naruse K, et al. Comparison of the cytokine-induced migratory response between primary and subcultured populations of rat mesenchymal bone marrow cells. *J Orthop Sci* 2007; 12: 484.
18. Vacanti V, Kong E, Suzuki G, et al. Phenotypic changes of adult porcine mesenchymal stem cells induced by prolonged passaging in culture. *J Cell Physiol* 2005; 205: 194.
19. Muguruma Y, Yahata T, Miyatake H, et al. Reconstitution of the functional human hematopoietic microenvironment derived from human mesenchymal stem cells in the murine bone marrow compartment. *Blood* 2006; 107: 1878.
20. Rombouts WJ, Ploemacher RE. Primary murine MSC show highly efficient homing to the bone marrow but lose homing ability following culture. *Leukemia* 2003; 17: 160.
21. Koide Y, Morikawa S, Mabuchi Y, et al. Two distinct stem cell lineages in murine bone marrow. *Stem Cells* 2007; 25: 1213.
22. Morikawa S, Mabuchi Y, Kubota Y, et al. Prospective identification, isolation, and systemic transplantation of multipotent mesenchymal stem cells in murine bone marrow. *J Exp Med* 2009; 206: 2483.
23. Chao PH, Grayson W, Vunjak-Novakovic G. Engineering cartilage and bone using human mesenchymal stem cells. *J Orthop Sci* 2007; 12: 398.
24. Sacchetti B, Funari A, Michienzi S, et al. Self-renewing osteoprogenitors in bone marrow sinusoids can organize a hematopoietic microenvironment. *Cell* 2007; 131: 324.
25. Nagaya N, Kangawa K, Itoh T, et al. Transplantation of mesenchymal stem cells improves cardiac function in a rat model of dilated cardiomyopathy. *Circulation* 2005; 112: 1128.
26. Ohori Y, Yamamoto S, Nagao M, et al. Growth factor treatment and genetic manipulation stimulate neurogenesis and oligodendrogenesis by endogenous neural progenitors in the injured adult spinal cord. *J Neurosci* 2006; 26: 11948.
27. Sata M, Saiura A, Kunisato A, et al. Hematopoietic stem cells differentiate into vascular cells that participate in the pathogenesis of atherosclerosis. *Nat Med* 2002; 8: 403.
28. Hou Z, Nguyen Q, Frenkel B, et al. Osteoblast-specific gene expression after transplantation of marrow cells: Implications for skeletal gene therapy. *Proc Natl Acad Sci USA* 1999; 96: 7294.

mTOR Immunosuppression in HIV-Positive Liver Transplant Recipients

We read with interest the article by Di Benedetto et al. (*1*) regarding their experience with rapamycin as the principal immunosuppressive drug in HIV-positive recipients of liver transplantation. The authors reported switching from calcineurin inhibitors (CNIs) to rapamycin in six patients mainly because of renal dysfunction (five of six) at a median of 67 days (range 10–225 days) from transplantation. The main message from this experience comes, however, from the data regarding HIV-RNA control in patients under rapamycin therapy. The authors reported that cases taking rapamycin had a better control of HIV-RNA replication than cases under CNIs, suggesting a possible antiretroviral effect of rapamycin. However, it is not clear to us why most of the patients taking CNIs have detectable HIV-RNA viral load because they are all actively taking antiretroviral therapy (ART), which was restarted, on average, 16 days after transplant (range 9–58 days) with at least three drugs in association, such as their counterparts on rapamycin treatment. In our personal experience (30 liver transplantations in HIV-infected patients), we were able to suppress HIV-RNA in all cases that were on ART after transplantation. What we would expect is that all cases under ART would have suppressed HIV-RNA viral load independently from the type of immunosuppression. In particular, we switched seven patients from CNIs to mammalian target of rapamycin (mTOR; three to rapamycin and four to everolimus) at a median of 17 months (range 11–22 months) after transplantation for renal impairment attributed to CNIs toxicity. All those cases, which were actively taking ART at the moment of switching from CNIs to mTOR, were already HIV-RNA negative and remained negative while on mTOR treatment. Therefore, on the basis of our experience, we would suggest that control of HIV-RNA viremia in liver transplanted patients is still a matter of the choice of the best ART independently from the type of the antirejection treatment; moreover, the use of rapamycin in this context may be misleading because it has been already clearly demonstrated that ART has an impact on overall survival in HIV-positive liver transplanted patients (*2*). A possible antiretroviral effect of an mTOR class of immunosuppressant, as hypothesized in the literature (*3–5*), should be investigated only in patients not taking effective ART for any reason after transplantation.

Umberto Baccarani[1]
Gian Luigi Adani[1]
Marcello Tavio[2]
Paolo Grossi[3]
Pierluigi Viale[4]

[1]Transplantation Unit
University of Udine
Udine, Italy

[2]Division of Infectious Diseases of Ancona
Ancona, Italy

[3]Institute of Infectious Diseases
University of Insubria
Varese, Italy

[4]Institute of Infectious Diseases
University of Bologna
Bologna, Italy

Address correspondence to: Umberto Baccarani, M.D., Ph.D., F.E.B.S., Transplantation Unit, University of Udine, Udine, Italy.
E-mail: umberto.baccarani@uniud.it

U.B. participated in research and wrote the article; G.L.A. participated in research; M.T. participated in research and reviewed the article; P.G. designed the study and reviewed the article; and P.V. designed the study and reviewed the article.
Received 28 May 2010.

Ultrasound in Med. & Biol., Vol. 36, No. 7, pp. 1098–1108, 2010

0301-5629/$–see front matter

ELSEVIER

doi:10.1016/j.ultrasmedbio.2010.04.011

● *Original Contribution*

PROLONGED ENDOCHONDRAL BONE HEALING IN SENESCENCE IS SHORTENED BY LOW-INTENSITY PULSED ULTRASOUND IN A MANNER DEPENDENT ON COX-2

KOUJI NARUSE,* HIDEKI SEKIYA,[†,1] YOSHIHUMI HARADA,[‡] SADAHIRO IWABUCHI,[‡,2] YUSUKE KOZAI,[§] RYOTA KAWAMATA,[§] ISAMU KASHIMA,[§] KENTARO UCHIDA,* KEN URABE,* KANNICHI SETO,[†] MORITOSHI ITOMAN,* and YUKO MIKUNI-TAKAGAKI[¶]

*Department of Orthopedic Surgery, Kitasato University School of Medicine, Sagamihara; [†]First Department of Oral and Maxillofacial Surgery, School of Dental Medicine, Tsurumi University, Yokohama; [‡]Bone and Joint Research Laboratories, Teijin Pharma Limited, Tokyo; [§]Department of Maxillofacial Diagnostic Science; and [¶]Department of Functional Biology, Kanagawa Dental College, Yokosuka, Japan

(*Received* 22 *September* 2009; *revised* 15 *March* 2010; *in final form* 19 *April* 2010)

Abstract—To test whether mechanical loading produces faster healing in aged mice, fractured femurs of aged 1-year-old mice were subjected to low-intensity pulsed ultrasound (LIPUS), a treatment that is routinely used to help heal fractures in humans. Cyclooxygenase-2 knockout mice (COX-2$^{-/-}$), which lack an immediate early mediator of mechanical stimulation, were also studied by histochemistry, microcomputed tomography and quantitative polymerase chain reaction to determine the role of COX-2. The healing in the aged COX-2$^{-/-}$ mice is slow during the endochondral bone remodeling (>30 d), a period generally prolonged in senescence. For aged wild-type mice, LIPUS halved the endochondral phase to about 10 d, whereas that was not the case for aged COX-2$^{-/-}$ mice, which showed no apparent shortening of the prolonged endochondral-phase healing time. Injecting prostaglandin E_2 receptor agonists, however, rescued the COX-2$^{-/-}$ callus from insensitivity to LIPUS. In conclusion, COX-2 is a limiting factor in the delayed endochondral bone healing and is induced by LIPUS, which normalizes healing rate to the wild-type level. (E-mail: yukomtak@kdcnet.ac.jp) © 2010 World Federation for Ultrasound in Medicine & Biology.

Key Words: **Cyclooxygenase-2 (COX-2), Prostaglandin E_2 (PGE_2), Fracture healing, Low-intensity pulsed ultrasound (LIPUS).**

INTRODUCTION

Fracture healing slows with age in rats (Ekeland et al. 1982) and humans (Nilsson and Edwards 1969). Recent investigation has shown that induced levels of COX-2 expression during the first postoperative week in the fracture callus of 1-year-old mice are only one-third of those of 8-week-old mice (Naik et al. 2009). Nonsteroidal antiinflammatory drugs (NSAIDs) and other COX-2 inhibitors have been reported to impair fracture healing in humans (Elmstedt et al. 1985; Sudmann and Hagen 1976) and animals (Bo et al. 1976). Significant osteogenic deficiencies were observed in rats aged 6–9 months that were administered indomethacin from the second postoperative week, whereas 2-month-old rats were not significantly affected (Elves et al. 1982). Thus, it was suggested that people who have fractured osteoporotic bone should avoid agents that inhibit COX-2 (Dinchuk et al. 1995).

Our previous studies established the role of COX-2 as a mechanical-response amplifier in primary rat bone cells and ST2 cells, a mouse stem cell line. COX-2 is an essential link in the process that sustains the anabolic effect of mechanical stimuli by amplifying the effect of the initial mechanical input as a result of biphasic secondary expression of COX-2 (Kawata and Mikuni-Takagaki 1998; Naruse et al. 2003). In fact, appropriate mechanical loading has a vital positive influence on skeletal healing (Augat et al. 2005). Therefore, to evaluate the efficacy of mechanical treatment with low-intensity pulsed ultrasound (LIPUS) in 1-year-old COX-2 knockout mice and their wild-type (WT) littermates, we examined their fracture calluses with and without LIPUS exposure.

Address correspondence to: Yuko Mikuni-Takagaki, Ph.D., Department of Science, Kanagawa Dental College, 82 Inaokacho, Yokosuka, Kanagawa 238-8580 Japan. E-mail: yukomtak@kdcnet.ac.jp

Present addresses: [1]Department of Oral Surgery, School of Medicine, Toho University, Tokyo and [2]Division of Immunoregulation, Institute for Genetical Medicine, Hokkaido University, Sapporo, Japan.

MATERIALS AND METHODS

Experimental design

We bilaterally fractured the femurs of aged (1-year-old) COX-$2^{-/-}$ mice and the WT littermates (COX-$2^{+/+}$). The right femur of each animal received a 20-min LIPUS treatment every day, starting on day 5, the fifth day after surgery (we define the day of surgery to be day 0). The left femurs served as controls and received mock treatment. Each group initially consisted of eight animals. In spite of the inherent risk of anesthesia, no more than two mice in each group died during these experiments. Three repeated experiments were performed. The time frame for the fracture healing of the aged mice, as well as that of skeletally mature, 10-week-old adult mice, is depicted in Fig. 1. The duration of endochondral bone formation is marked with double-headed arrows on a solid gray line for WT mice and a dotted gray line for the knockout mice.

To confirm whether prostaglandin E_2 (PGE_2) receptor agonists restore signals in response to LIPUS missing in old COX-$2^{-/-}$ mouse callus, we attempted a rescue experiment in which the bilateral femurs of the eight experimental knockout mice were fractured and treated with the EP-2 and EP-4 PGE_2 receptor agonists starting on day 5, the end of the inflammation stage, to day 21. Control COX-$2^{-/-}$ mice received vehicle solution. The right femur of each animal received a 20-min LIPUS treatment every day, starting on day 5.

Mice

The Animal Care and Use Committee of Kanagawa Dental College approved our experimental protocol. We used 48 mice. All mice were the hybrid C57BL/6J×129S7 (B6, 129S7-Ptgs2tm1Jed; The Jackson Laboratory, Bar Harbor, ME, USA) (Dinchuk et al. 1995), having been intercrossed for ~30 generations at Kanagawa Dental College. In addition to the knockout mice and the WT littermates, some heterozygous mice (COX-$2^{+/-}$) for the COX-2 gene were also used to histologically compare the healing rates.

Fractures

We anesthetized all mice with 80 mg/kg ketamine and 16 mg/kg xylazine and performed a medial parapatellar arthrotomy to insert a 26g needle into the medullary canal of the one or both femurs. After the exposed portion of the needle was cut off, the patella was replaced and the incision was sutured with 8-0 synthetic absorbable stitches. The stabilized femur was fractured manually at the midpoint of the diaphysis (Bonnarens and Einhorn 1984). Fracture healing was monitored by soft X-ray contact micrography (HA-60 system, Hitex Co., Osaka, Japan) of the femora of anesthetized mice with Industrial X-ray film IX FR (Fuji Photo Film Co. Ltd., Tokyo, Japan).

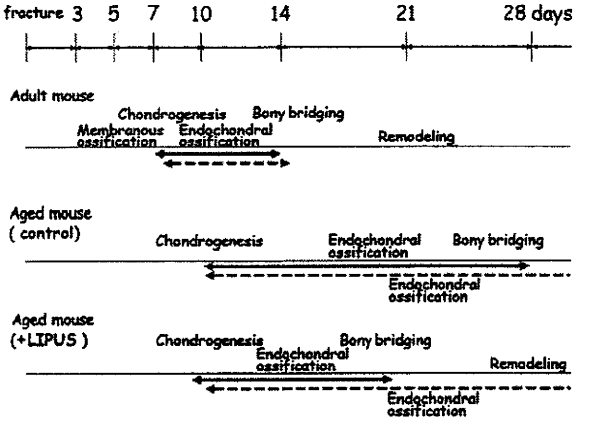

Fig. 1. Schematic representation of sequence of fracture healing processes in adult (10-week-old) and aged (1-year-old) mice. *Filled arrows* represent endochondral ossification stage in WT mice, and *dotted arrows* in COX-$2^{-/-}$ mice. Healing processes proceeded similarly in the 10-week-old COX-$2^{-/-}$ and the WT mice (See Supplementary Fig. S1 for radiographs).

Ultrasound treatment

A device equipped with six lead zirconate titanate transducers 13 mm in diameter (Teijin, Tokyo, Japan) applied LIPUS to the experimental fractures. The six transducers were connected to a generator through six separate lines with individual switches. A function generator (model HP33120A; Hewlett-Packard Japan, Ltd., Tokyo, Japan) produced a 200-μsec burst of 1.5-MHz sine waves repeated at 1.0 KHz at a spatial average and temporal average intensity of 30 mW/cm^2. These transcutaneous LIPUS parameters are identical to those used in human therapy (Fujioka et al. 2000), in experiments with rodents (Azuma et al. 2001) and in experiments with bone-cell cultures (Naruse et al. 2000, 2003). During treatment, the mice were anesthetized to aim the ultrasound to the fracture site with a subcutaneous injection of ketamine (80 mg/kg) and xylazine (16 mg/kg) and kept in a prone position on cylindrical holders with transducers placed close to the skin at the femoral fracture site, which was shaved and covered with ultrasound gel (Nippon Kohden, Tokyo, Japan) (Azuma et al. 2001). Control animals were also anesthetized and had transducers attached to the fracture site, but the transducers were not connected to the ultrasound generator.

Microfocused X-ray computed tomography

Microfocused X-ray computed tomography (micro-CT) equipped with a microfocus X-ray tube (focus size 8 × 8 μm, MCT-100MF, Hitachi Medical Corporation, Tokyo, Japan) produced a 3-D image of each femur from 200 image slices. The tube voltage, tube current,

magnification, and voxel size were 70 kV, 100 mA, x7 and 17.8 × 17.8 × 17.8 micrometers, respectively. Using TRI/3D BON software (Ratoc System Engineering Co. Ltd., Tokyo, Japan), 3-D structural parameters such as bone volume (BV, mm^3), bone surface (BS, mm^2), bone volume fraction (BV/TV, %), trabecular thickness (Tb.Th, μm), trabecular number (Tb.N, 1/mm) and trabecular separation (Tb.Sp, μm) were calculated (Ruegsegger et al. 1996). For the bone regions, we separated trabecular bone from cortical bone by 3-D space filtration; data from the each slice were converted to binary data using a threshold obtained by a discriminant analysis in which the pixel value histograms of background and bone were assumed to be normally distributed. We then chose each threshold as an intermediate pixel value lying on the tails of the two normal distributions.

Tissue preparation

For histochemical studies, resected calluses were immediately treated with 10% formalin at 0 °C, immersed overnight in fresh formalin and decalcified in 3M ethylenediamine tetraacetic acid for 2–3 weeks. Undecalcified 7-μm sections were prepared by embedding the callus in 2-hydroxyethylmethacrylate (GMA) and staining with classical hematoxylin/eosin, Goldner's trichrome or Toluidine blue.

Message levels in fracture calluses

Some fracture calluses were exposed to LIPUS for 20 min on days 6 and 7, 24 h apart. Femurs, both experimental and control, were excised 30 min after the last LIPUS exposure and immediately placed in RNA Later (Ambion, Austin, TX, USA). After dissection under a stereomicroscope, calluses were pulverized with a stainless steel mortar and pestle that had been chilled in liquid N_2 (Cryo-Press crusher; Microtec, Funabashi, Japan). Pulverized tissue was collected into a reagent containing phenol and guanidinium isothiocyanate to recover RNA. Total RNA was separated by centrifugation in Phase Lock Gel tubes (Eppendorf, Hamburg, Germany) after mixing with chloroform. Aliquots of 5 μg of recovered RNA were reverse-transcribed. The product cDNA was normalized with glyceraldehyde-3-phosphate dehydrogenase and subjected to conventional polymerase chain reaction (PCR) or real-time qPCR (QuantiTect SYBR Green PCR reagent kit; Qiagen, Hilden, Germany). Primer sequences are available upon request.

Injection of EP-2/EP-4 receptor agonists

From days 6–21, we subcutaneously injected two receptor agonists daily near the fracture callus in eight mice. The daily dose included 5 μg/kg of ONO-AE1-259-01, an EP-2 receptor agonist, dissolved in ethanol at 0.5 mg/mL and 5 μg/kg of ONO-AE1-329, an EP-4 receptor agonist, dissolved in water at 1 mg/mL. Both of these (a kind gift from Ono Pharmaceutical, Osaka, Japan) were further diluted to 5 μg/mL each in physiological saline solution containing 0.1% (w/v) Tween 80. Animals received 50 to 60 μL depending on body weight.

Statistical analysis

Relative values for the callus mRNAs are presented as the means ± SD for 6–8 rats in each group. Given the broad range of values detected among specimens from different calluses and different genetic groups, values relative to that of day 7 WT control callus in the same set of experiments were subjected to statistical analysis by Dennett's test with day 7 WT control value as a reference. Probability values less than 0.05 were considered significant. Because of the extremely low level on day 7 in WT control callus (VEGFa and MMP-3) and in KO callus (MMP-3), the results for VEGFa and MMP-3 are expressed without significance.

RESULTS

Fracture healing for aged mice

In the soft-X-ray profiles of femora of live and anesthetized 1-year-old mice taken on days 21 and 49, the blind observers detected differences between the profiles of knockout mice and those of WT mice (Fig. 2A). By day 49, all fractures in WT animals had reached union, whereas none of the fractures in knockout mice had done so. At both 21 d and 49 d, there was noticeably less healing of fractures in knockout mice than in WT mice. The fracture healing rate for heterozygotes (COX-$2^{+/-}$, Fig. 2A, c and d) was less than that of WT mice (Fig. 2Ae and 2Af) and greater than that of knockout mice (Fig. 2Aa and 2Ab). No less healing of fractures is present with younger, 10-week-old adult COX-$2^{-/-}$ mice (Supplementary Fig. S1 for comparison).

Effect of LIPUS on the rate of fracture healing in the aged mice

In the right femora of day 21 aged mice, Goldner's trichrome staining showed that LIPUS treatment from days 5–21 accelerated healing in both WT mice, which shifted from the endochondral ossification phase into the remodeling phase to cortical bone (Fig. 2Be to 2Bf), and the heterozygous COX-$2^{+/-}$ mice, which shifted from the bony callus phase with a fracture gap to the bony bridging phase by continuous woven bone (Fig. 2Bc to 2Bd).

In contrast, LIPUS is apparently ineffective for bony bridging in the healing of the COX-$2^{-/-}$ knockout mouse; Fig. 2Bb and 2Ba presented similar gaps at the fracture sites without being connected by woven bone. It should be noted that red staining represents the areas of soft tissue

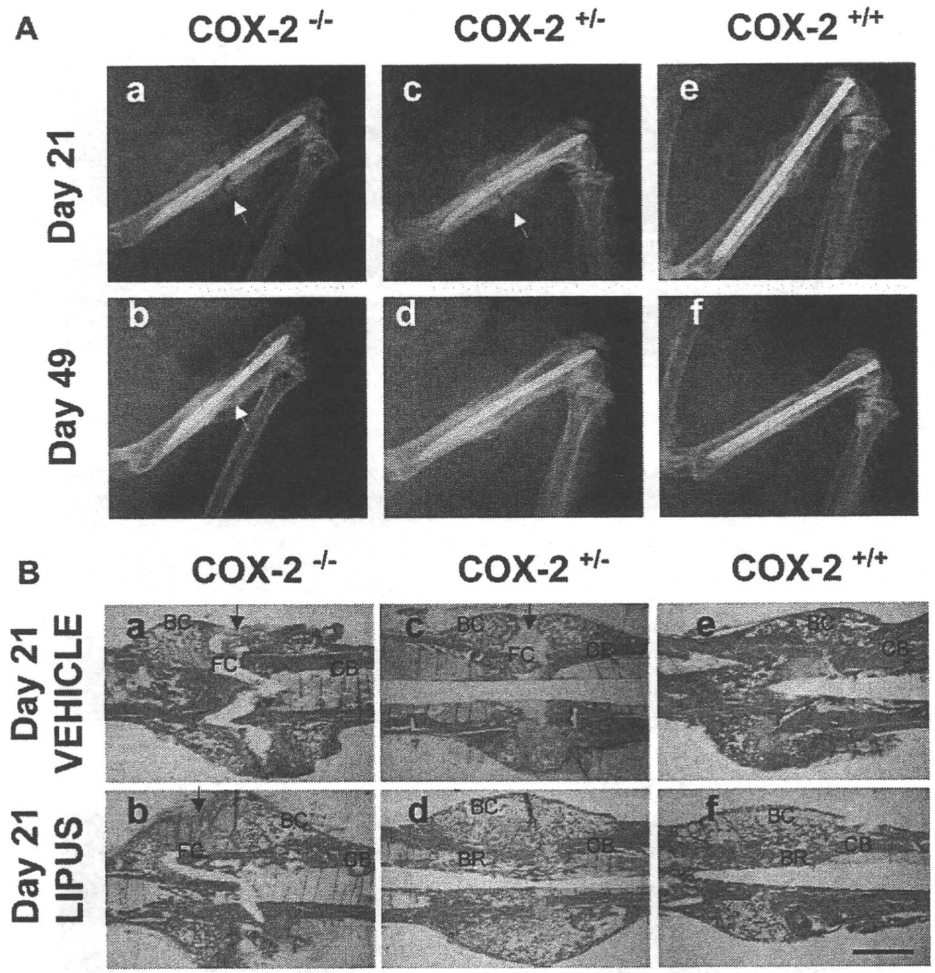

Fig. 2. Representative soft X-ray profiles (A) and histochemical profiles (B) of postfracture femurs of 1-year-old homozygous COX-2 knockout (COX-$2^{-/-}$), heterozygous (COX-$2^{+/-}$) and WT (COX-$2^{+/+}$) mice. (A) Day 21 (a, c, e) and day 49 (b, d, f) results are compared. (B) The day 21 postfracture femurs were either treated with LIPUS (b, d, f) or vehicle-treated (a, c, e). Undecalcified resin sections were visualized by Goldner's trichrome staining as described in Materials and Methods. Before the bony bridging typically observed in f and d, the edges of the newly formed woven bone are separated by the soft tissue as shown in a, b and c. FC, fibrous callus; BC, bony callus; CB, cortical bone; BR, area of bone remodeling. Scale bar represents 1 mm. Arrows in (A) and (B) indicate the fracture gaps filled with fibrous materials.

and slightly mineralized woven bone, and blue staining represents cortical bone. Calluses were further studied by Toluidine blue staining, which shows cartilage as purple, on earlier days 10 and 21. Chondrogenesis is at its peak and endochondral bone formation starts at about day 10 in aged normal mice. COX-$2^{-/-}$ and COX-$2^{+/+}$ calluses showed that cartilage formation in the knockout mice was essentially normal up to day 10 (Fig. 3Aa similar to 3Ac). However, exposure to LIPUS, which markedly accelerated endochondral replacement of cartilaginous tissue by woven bone in WT fractures (Fig. 3Ad *vs.* 3Ac), did not affect knockout fractures (Fig. 3Ab similar to 3Aa, rather than to 3Ad). By day 21, in control WT callus, most cartilage had been replaced by woven bone (Fig. 3Bc). LIPUS exposure accelerated remodeling furthermore by resorption of woven bone and cortical bone recovery (Fig. 3Bd). In knockout mice, however, endochondral bone formation was stunted, and cartilage was still apparent on day 21 (Fig. 3Ba). Even with LIPUS treatment, gaps filled with fibrous material persisted and prevented bony bridging (Fig. 3Bb). Overall, only in the presence of COX-2, LIPUS halved the interval needed for the endochondral bone formation of aged mice judged by the landmarks of healing, which is summarized in Fig. 1.

For the structural analysis of the newly formed bone, we obtained micro-CT scans of the femora on day 21. These image sets show the microstructural differences between fractures in knockout mice and those in their wild-type littermates, both with and without LIPUS (Fig. 3C). In the COX-$2^{-/-}$ femora, no bridging of bony callus was seen and fracture gaps

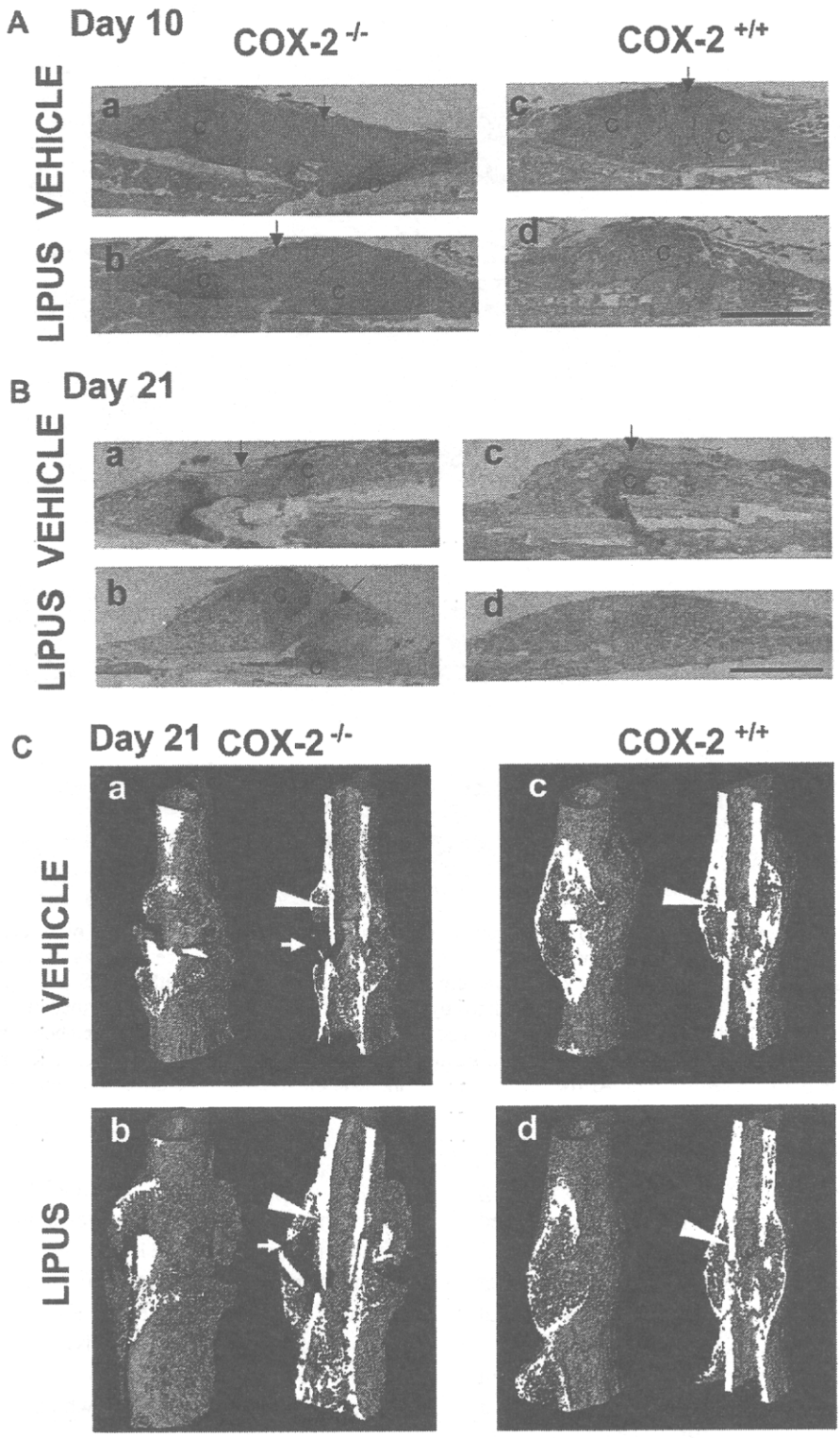

Fig. 3. Histochemical evaluation of fracture healing of 1-year-old mouse femora. (A) Toluidine blue staining profiles of day 10 postfracture femora of knockout mice (COX-$2^{-/-}$, a and b) and WT littermates (COX-$2^{+/+}$, c and d) were either LIPUS-exposed (b and d) or vehicle-treated (a and c). *Dotted lines* indicate the border of cartilaginous and fibrous callus. Chondroitin sulfate in cartilage (c) is stained purple. Scale bar: 1 mm. (B) Toluidine Blue staining profiles on day 21 under the same conditions as in Fig. 3A. (C) 3-D reconstruction of micro-CT profiles from day 21 postfracture femora of 1-year-old knockout mice (COX-$2^{-/-}$, a and b) and wild-type littermates (COX-$2^{+/+}$, c and d), either LIPUS-exposed (LIPUS, b and d) or vehicle-treated (Vehicle, a and c). Projections of reconstructed femora are depicted as projected at 30° clockwise to the frontal plane. Tomograms (*right*) and aspects (*left*) were reconstructed for representative femora. *Arrows* in (A), (B) and (C) indicate the fracture gaps, and the arrowheads in (C) represent the area of woven bone analyzed in Table 1.

were apparent regardless of LIPUS. At the fracture line, the bony callus curled inward, leaving a gap between the blunt ends of woven bone. In day 21 images of WT mice, however, healing had progressed such that the fracture line was undetectable and the periosteal membranous bone, as well as the woven bone, had fully bridged the fracture. Furthermore, LIPUS treatment markedly accelerated union of newly formed cortical bone, woven bone having mostly been resorbed by day 21 (Fig. 3Cd). Micro-CT analysis of the area of woven bone confirmed, on the basis of decreased BV/TV, trabecular thickness and increased trabecular separation, that resorption had progressed in mice exposed to LIPUS (Table 1). The BV/TV value, for example, was 26.2 ± 1.4% (see the area of woven bone indicated by an arrowhead in Fig. 3Cc) in the WT control callus, whereas the remaining woven bone in the LIPUS-exposed, resorbed callus (Fig. 3Cd equivalent to Fig. 3Bd) was 20.8 ± 0.3%. In contrast, in day 21 images of the femora of knockout mice, LIPUS brought little apparent change; cartilage and the fracture gap persisted. There was, however, a thickening of woven bone (Fig. 3Bb and 3Cb *vs.* 3Ba and 3Ca) that correspond to the micro-CT data of increased BV/TV, 26.4 ± 1.4% *vs.* 21.1 ± 0.7%; increased trabecular number, 8.1 ± 0.6 mm^{-1} *vs.* 6.4 ± 0.5 mm^{-1}; and decreased trabecular separation, 91.0 ± 8.9 μm *vs.* 123.1 ± 11.0 μm (Table 1). These values in the LIPUS-exposed knockout callus just happened to be similar to the WT vehicle value.

Bone and cartilage-protein expression in callus

To further delineate the mechanisms causing the slower healing rate, we selected messages that characterize bone healing. Dissected calluses were subjected to reverse transcriptase–PCR. By comparing results of basal day 7 (Fig. 4A, lane D7), day 7 after LIPUS (lane D7US) and basal day 10 (lane D10), the effect of LIPUS was evaluated in the normal course of events. In Fig. 4Aa1–4Aa3, levels of Col1a1, Col2a1, osterix, alkaline phosphatase (ALP), aggrecan and BMP-6 all increased in the order D7≤D7US<D10 (for Runx2 in Fig. 4A, b, D7<D7US≒D10). MMP-13 and osteocalcin showed similar profiles (data not shown). The order for the level of MMP-9 was reversed (Fig. 4Ac, D7≥D7US≥D10). On the other hand, WT D7US MMP-2 level was much higher with LIPUS than D7 and D10 basal levels (Fig. 4Ad, D7US>D7≒D10; TGF-α1 was similar). D7US levels of Col10a1, BMP-2, BMP-4, FGF-2, VEGFa, MMP-3, COX-2 and RANKL were also higher than both D7 and D10 basal levels (Fig. 4Ae to 4Ah). Compared with these LIPUS-specific WT responses in 4Ad–4Ah, Col3a1 and COX-1 remained constant throughout (Fig. 4Ai). In COX-$2^{-/-}$ callus on day 7 (Fig. 4B), in contrast, loss of detectable messages was observed for VEGFa, ALP and MMP-9 (TGF-α2 and RANKL showed similar results), regardless of LIPUS (Fig. 4Ba). In BMP-6, as well as MMP-2 and aggrecan, lower levels of expression were detected in the knockout callus, especially with LIPUS (WT>KO>KOUS, Fig. 4Bb). BMP-2, COL1a1, COL1a2 and COL3a1, as well as Runx2 and osterix messages in COX-$2^{-/-}$ mouse callus, showed similar levels to the WT day 7 levels (Fig. 4Bc). MMP-3 (Fig. 4Bd), Col10a1 and possibly TGF-α1and BMP-4 (Fig. 4Be) increased the messages in knockout callus, especially after LIPUS exposure (WT<KO<KOUS). The level of FGF-2 message in the knockout mouse was higher than the WT but showed no further elevation by LIPUS (WT<KO≒* KOUS in Fig. 4Bf).

Rescue from deficient healing with EP-2/EP-4 receptor agonists

Micro-CT profiles and parameters show that the 1-year-old COX-$2^{-/-}$ mice healed just as well as their WT littermates if EP-2 and EP-4 receptor agonists were present. Table 2 and Fig. 5, compared with Table 1 and Figs. 3 and 4, showed the regained WT-level response to LIPUS in addition to the recovery of parameters to the WT levels in EP-2/EP-4–treated COX-$2^{-/-}$ mice callus; Fig. 5Ab and 5Bb *vs.* 5Aa and 5Ba are equivalent

Table 1. Effects of LIPUS on structural parameters of newly formed woven bone in the external callus analyzed in the day 21 fractures by 3-D micro-CT

	WT littermates		Knockout	
Variable	Vehicle	LIPUS	Vehicle	LIPUS
BS/BV 1/mm	61.4 ± 2.9	65.1 ± 2.3*†	60.7 ± 2.8	61.2 ± 1.6
BV/TV%	26.2 ± 1.4	20.8 ± 0.3*†	21.1 ± 0.7*	26.4 ± 1.4†
Tb.Th μm	32.6 ± 0.9	30.8 ± 1.4*†	32.8 ± 1.5	32.6 ± 0.8
Tb.N 1/mm	8.1 ± 0.8	6.8 ± 0.2	6.4 ± 0.5*	8.1 ± 0.6†
Tb.Sp μm	91.6 ± 8.0	116.9 ± 2.9*†	123.1 ± 11.0*	91.0 ± 8.9†
Fractal dimension	2.25 ± 0.0	2.19 ± 0.0	2.31 ± 0.06	2.31 ± 0.01

Wild-type (Cox-$2^{+/+}$) and COX-2KO (Cox-$2^{-/-}$) mouse calluses were subjected to the analysis.

Values are mean ± SD. Within each variable, significance was compared with vehicle for the WT mice (*$p < 0.05$), and within each genotype, significance was compared with LIPUS-untreated vehicle mice (†$p < 0.05$) by the two-tailed multiple *t*-test with Bonferroni correction (4 comparisons in 4 groups).

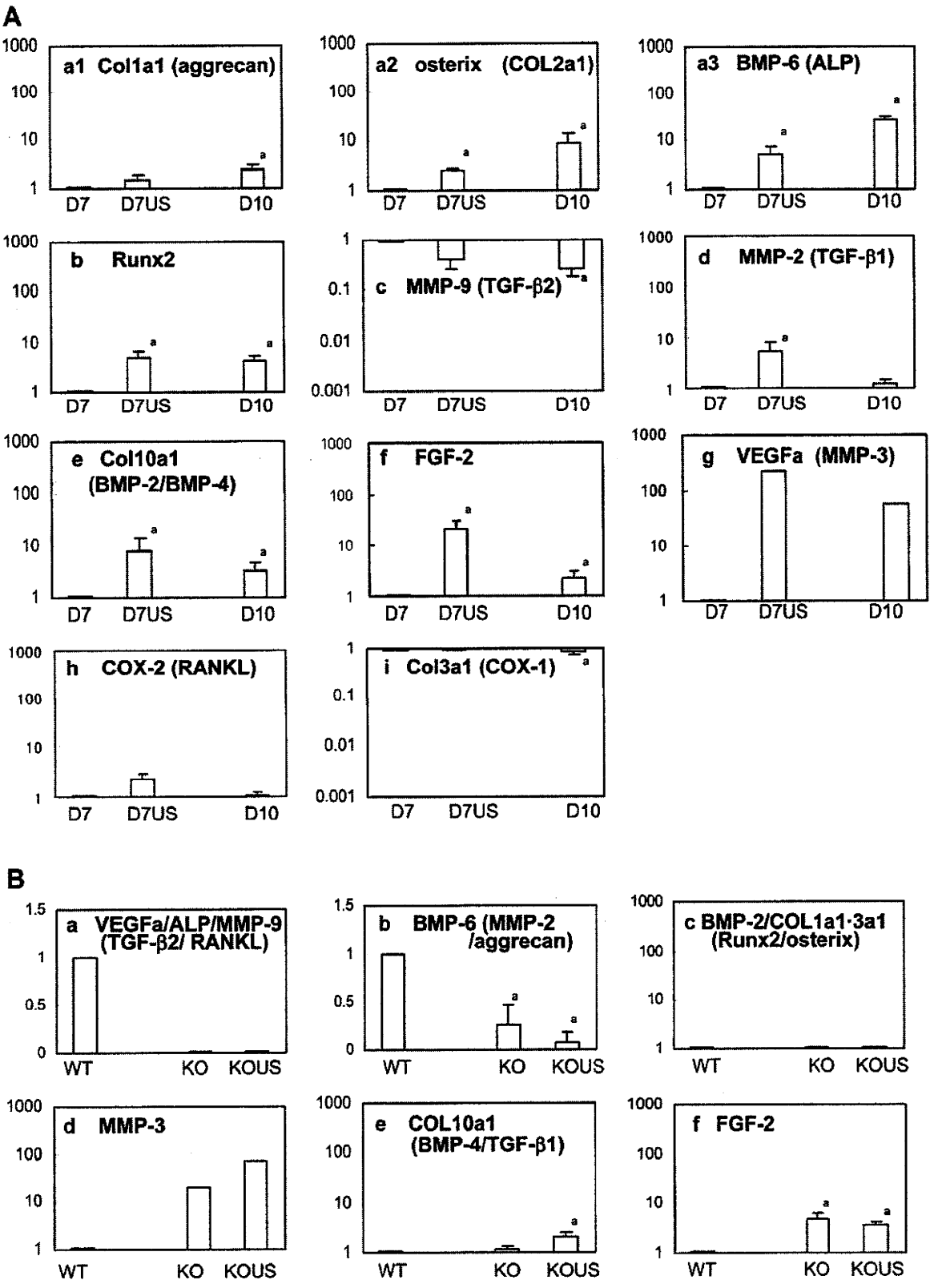

Fig. 4. Transcript levels in the fracture callus of 1-year-old mice. (A) WT littermates, D7, D7US and D10, at 7 or 10 d post-fracture. D7US samples were from day 7 femurs exposed to LIPUS; D7 and D10, vehicle-treated controls from day 7 and day 10 femurs. Total RNA was extracted from the dissected callus and subjected to quantitative reverse transcriptase–PCR as described in Materials and Methods. In a1, Col1a1 (similar to aggrecan); a2, osterix (similar to Col2a1) a3, BMP-6 (similar to ALP); b, Runx2; c, MMP-9 (similar to TGF-α2); d, MMP-2 (similar to TGF- α1); e, Col10a1 (similar to BMP-2 and BMP-4); f, FGF-2; g, VEGFa (similar to MMP-3); h, COX-2 (similar to RANKL); i, Col3a1 (similar to

to Fig. 3Bd and 3Cd *vs.*3Bc and 3Cc, and Fig. 5C is equivalent to Fig. 4Ag.

DISCUSSION

Although LIPUS accelerates the healing process for WT 1-year-old mice, it does not do so for their COX-$2^{-/-}$ littermates. The significantly retarded fracture healing rate we observed for aged COX-$2^{-/-}$ mice during the endochondral ossification accords well with previously published reports that NSAIDs and other COX inhibitors slowed down the fracture healing process in adult rats and humans (Allen et al. 1980; Bo et al. 1976; Elmstedt et al. 1985; Sudmann and Hagen 1976) and that a single local application of a retroviral vector expressing a single COX-2 transgene accelerated fracture healing in aged rats (Rundle et al. 2008).

Because the healing milestones during and after the endochondral bone formation are essentially the same for 10-week-old COX-$2^{-/-}$ as they are for their WT littermates (see summary in Fig. 1 and Supplementary Fig. S1), the question to be asked is what function COX-2 and its product PGE_2 perform in fracture healing, specifically in older animals. Keller et al. (1993) observed significant stimulation of endochondral remodeling into bone after infusing PGE_2 into 9-month-old rabbits from weeks 3–6 postfracture. However, no significant difference was observed if the same infusion was given during the first three weeks. They suggested that PGE_2 is scarce and that if artificially infused in later weeks, it effectively promotes remodeling. In our present experiment, LIPUS exposure accelerated the rate of endochondral remodeling in the aged WT mice. Although COX-2 may not be the sole determinant of fracture healing, mechanical stimulation such as LIPUS increases the amount or level of PGE_2 in aged individuals as a result of an increase in COX-2, which is induced in mechanically stimulated osteoblasts (Forwood 1996; Naruse et al. 2003). Feedback upregulation of COX-2 by the product, PGE_2 (Kawaguchi et al. 1994), explains the long-lasting effect of exercise on PGE_2 production and bone formation (Forwood 1996; Naruse et al. 2003).

Previous *in vivo* studies have demonstrated that LIPUS affects all phases of the healing process in rats and that LIPUS shortens the healing period in patients (Azuma et al. 2001; Nelson et al. 2003). Yang et al. (1996) reported in adult rats a biphasic shift in aggrecan gene expression to a significantly higher level on day 7 and a lower level on day 21. These changes are anticipated if the effect of LIPUS on aggrecan gene is the result of attaining earlier landmarks and final union. In LIPUS-treated WT callus, we detected increases in ALP, Col2a1, aggrecan, Runx2, osterix and many other differentiation markers in the order D7<D7US≦D10, or decreases in the same order (MMP-9 and TGF-α2). Such changes induced by LIPUS are as anticipated in the due course of time and may have been attained by increasing circulation (Rawool et al. 2003) or slightly raising body temperature (Reuter et al.1984). In contrast, we discovered more specific effects provably dependent on each promoter in other genes of distinct behavior. Col10a1, BMP-2 and BMP-4 responded more specifically to LIPUS, judging from the higher levels of D7US than both D7 and D10 basal levels. MMP-2, MMP-3, TGF-α1, FGF-2, VEGFa, COX-2 and RANKL were elevated solely by LIPUS, suggestive of the specific target genes for specific healing effects. It should be noted that LIPUS specifically induces RANKL, which is essential to osteoclastogenesis and bone resorption (Tsukii et al.1998) and is not induced in COX-$2^{-/-}$ mouse callus. We found that LIPUS triggers additional metabolic turnover in fracture callus, even in aged mice, as long as PGE_2 is available. In COX-$2^{-/-}$ mice, lack of many such critical angiogenic and/or catabolic components as VEGFa and MMP-9 (Colnot et al. 2003; Engsig et al. 2000; Gerber et al. 1999), which have been reported being downstream of PGE_2 (Callejas et al. 2001; Gallo et al. 2001), prevents matrix degradation and remodeling in the healing bone. Fibroblastic Col3a1 messages, as well as those of Col1a1, remained constant in COX-$2^{-/-}$ callus, further supporting our observation of persistent mesenchymal tissue in the COX-$2^{-/-}$ fracture gaps regardless of LIPUS. In contrast to these mostly unaffected matrix proteins, Col10a1, BMP-4, TGF-α1 and possibly MMP-3 were upregulated in the COX-$2^{-/-}$ callus by LIPUS, suggesting certain compensatory alternative pathway(s) independent of COX-2. In addition, COX-$2^{-/-}$ callus showed persistent higher levels of FGF-2, which was reported to stimulate proliferation of fibroblasts and chondrocytes and to prolong the cartilaginous callus phase (Nakajima et al. 2001).

With regard to early-phase responses, Street et al. (2001) reported elevated VEGF and platelet-derived

COX-1). (B) Knockout mice, KO and KOUS, and WT littermates, WT, which is identical to D7 in (a), all at postfracture day 7. KO and WT values are basal controls. Panels a, VEGFa, ALP and MMP-9 (similar to TGF-α2 and RANKL); b, BMP-6 (similar to aggrecan and MMP-2); c, BMP-2, Col1a1, Col2a1and Col3a1 (similar to Runx2 and osterix); d, MMP-3; e, Col10a1 (similar to BMP-4 and TGF-α1); f, FGF-2. Data in (A) and (B) are expressed as the means ± SD. [a] Significant at $p < 0.05$ by Dennett's test with day 7 WT control values, D7 in (A) and WT in (B), as references. Fig. 4Ag and 4Bd, which have extremely low D7/WT values, are presented without SD values as described in Materials and Methods.

Table 2. Effects of LIPUS on structural parameters of newly formed woven bone in the external callus analyzed in the day 21 fractures by 3-D micro-CT

	WT littermates*		Knockout with EP2/EP4 agonists	
Variable	Vehicle	LIPUS	Vehicle	LIPUS
BS/BV 1/mm	61.4 ± 2.9	65.1 ± 2.3†‡	61.9 ± 0.7	70.7 ± 5.2†‡
BV/TV%	26.2 ± 1.4	20.8 ± 0.3†‡	27.1 ± 2.2	21.1 ± 2.5†‡
Tb.Th μm	32.6 ± 0.9	30.8 ± 1.4†‡	32.2 ± 0.4	28.2 ± 1.8†‡
Tb.N 1/mm	8.1 ± 0.8	6.8 ± 0.2	8.4 ± 0.6	7.5 ± 1.3
Tb.Sp μm	91.6 ± 8.0	116.9 ± 2.9†‡	86.7 ± 8.8	105.4 ± 4.2†‡
Fractal dimension	2.25 ± 0.0	2.19 ± 0.0	2.27 ± 0.01	2.30 ± 0.06

Results of COX-2 KO mice administered EP2 and EP4 agonists and of WT littermates were subjected to the analysis.

Values are mean ± SD. Within each variable, significance was compared with vehicle for the WT mice ($^{\dagger}p < 0.05$), and within each genotype, significance was compared with LIPUS-untreated vehicle mice ($^{\ddagger}p < 0.05$) by the two-tailed multiple *t*-test with Bonferroni correction (4 comparisons in 4 groups).

*Data from Table 1.

growth factor (PDGF) levels in plasma and fracture hematoma in fracture patients irrespective of age. Some other mechanisms must be sought, they wrote, for delayed union in elderly people. Also in rats, Meyer et al. (2001) reported transient upregulation of BMPs and PDGF immediately after fracture, regardless of age. We detected many specifically elevated genes in LIPUS-treated callus of 1-year-old WT mice that support the potential for aged mouse callus to respond to other types of mechanical stimulation as well. In the presence of COX-2, induced VEGFa will cause osteoblastic cells to differentiate, as reported by others (Peng et al. 2002; Street et al. 2002). Colnot et al. (2003) demonstrated that union is delayed in MMP-9 knockout mice and that MMP-9 mediates vascular invasion of cartilaginous callus. Absence of MMP-9 is responsible for the lack of VEGF

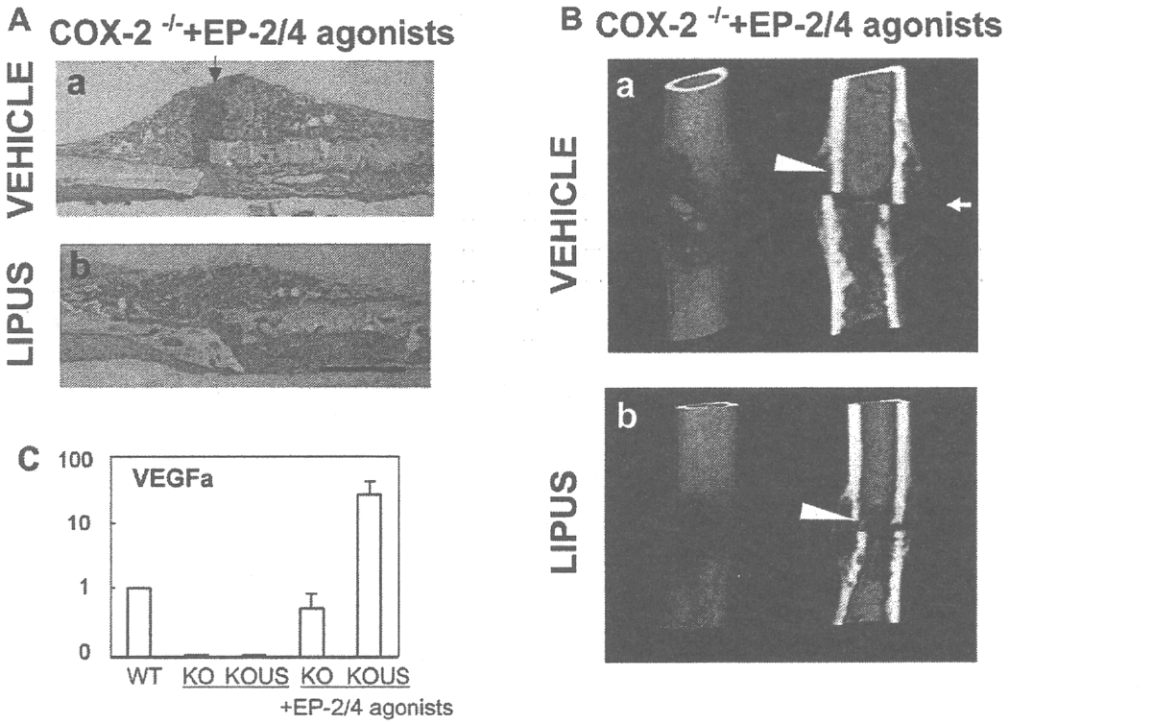

Fig. 5. Effects of EP-2 and EP-4 agonists and LIPUS on fracture callus of 1-year-old COX-2 knockout mouse femur. Histochemical (A) and micro-CT (B) profiles of callus with daily injections of agonists alone (a, Vehicle, from left femur) or with agonists and LIPUS exposure (b, LIPUS, from right femur). Daily treatments, started after 5 d postfracture, were continued through day 21. In (A) and (B), experimental conditions and markers in the figure are similar to those presented in Fig. 3. (C) Recovered expression of VEGFa in COX-$2^{-/-}$ fracture callus treated with EP-2/EP-4 agonists. Samples were analyzed under similar conditions to those described in Fig. 4 and relative values to that of the basal WT callus (WT) are presented.

bioavailability (Bergers et al. 2000). In COX-$2^{-/-}$ mice, neither VEGFa nor MMP-9 messages were detectable regardless of LIPUS. COX-2 is a ubiquitous upstream regulator of MMP-2, MMP-9, VEGF (Callejas et al. 2001; Gallo et al. 2001) and RANKL (Tsukii et al. 1998). Thus, our results underline the inability of COX-$2^{-/-}$ mice to use these molecules in fracture callus, even when mechanically stimulated.

COX-2 is essential in later stages of fracture healing in aged mice; cartilage and bone formation progress quasinormally in knockout mice up to day 10, and then they slow down. Recovery to the WT level was attained by injecting EP-2/EP-4 agonists after day 5. It is apparent that cells regained responsiveness to LIPUS. This COX-$2^{-/-}$ experiment to rescue normal bone formation and resorption, LIPUS-induced as well as basal, shows that the loss of COX-2–derived PGE_2 deters the endochondral remodeling of fractures in aged mice. It is possible that mechanical stimulation, which provides PGE_2 through COX-2 induction (Kawata and Mikuni-Takagaki 1998; Naruse et al. 2003), is less in aged mice than in younger mice during the endochondral remodeling phase of fracture healing. Elderly people receiving long-term NSAID therapy may have a slower healing rate because of the blockade of signal transduction downstream of mechanical loading, which favors skeletal healing (Augat et al. 2005).

Acknowledgments—We thank Kazuaki Miyagawa, presently at Osaka University Graduate School of Dental Medicine for technical assistance; Koji Tomimori and Dr. Yoshiaki Azuma, Teijin Pharma, for helpful discussions; and Dr. Ikuya Matsubara, Department of Science, Kanagawa Dental College for advice on the statistical analysis. This investigation was supported in part by grants-in-aid from the Ministry of Science, Education, and Culture of Japan to Y. M.-T. and H. S.; by grants-in-aid from the Ministry of Health, Labor, and Welfare for Research on the Human Genome, Tissue Engineering, and Food Biotechnology, to M. I.; and by a research support grant from Kanagawa Odontological Society to Y. M.-T.

SUPPLEMENTARY DATA

Supplementary data associated with this article can be found, in the online version, at doi:10.1016/j.ultrasmedbio.2010.04.011.

REFERENCES

Allen HL, Wase A, Bear WT. Indomethacin and aspirin: Effect of nonsteroidal anti-inflammatory agents on the rate of fracture repair in the rat. Acta Orthop Scand 1980;51:595–600.

Augat P, Simon U, Liedert A, Claes L. Mechanics and mechano-biology of fracture healing in normal and osteoporotic bone. Osteoporos Int 2005;16(Suppl. 2):S36–S43.

Azuma Y, Ito M, Harada Y, Takagi H, Ohta T, Jingushi S. Low-intensity pulsed ultrasound accelerates rat femoral fracture healing by acting on the various cellular reactions in the fracture callus. J Bone Miner Res 2001;16:671–680.

Bergers G, Brekken R, McMahon G, Vu TH, Itoh T, Tamaki K, Tanzawa K, Thorpe P, Itohara S, Werb Z, Hanahan D. Matrix metalloproteinase-9 triggers the angiogenic switch during carcinogenesis. Nat Cell Biol 2000;2:737–744.

Bo J, Sudmann E, Marton PF. Effect of indomethacin on fracture healing in rats. Acta Orthop Scand 1976;47:588–599.

Bonnarens F, Einhorn TA. Production of a standard closed fracture in laboratory animal bone. J Orthop Res 1984;2:97–101.

Callejas NA, Casado M, Diaz-Guerra MJ, Bosca L, Martin-Sanz P. Expression of cyclooxygenase-2 promotes the release of matrix metalloproteinase-2 and -9 in fetal rat hepatocytes. Hepatology 2001;33:860–867.

Colnot C, Thompson Z, Miclau T, Werb Z, Helms JA. Altered fracture repair in the absence of MMP9. Development 2003;130:4123–4133.

Dinchuk JE, Car BD, Focht RJ, Johnston JJ, Jaffee BD, Covington MB, Contel NR, Eng VM, Collins RJ, Czerniak PM. Renal abnormalities and an altered inflammatory response in mice lacking cyclooxygenase II. Nature 1995;378:406–409.

Ekeland A, Engesoeter LB, Langeland N. Influence of age on mechanical properties of healing fractures and intact bones in rats. Acta Orthop Scand 1982;53:527–534.

Elmstedt E, Lindholm TS, Nilsson OS, Tornkvist H. Effect of ibuprofen on heterotopic ossification after hip replacement. Acta Orthop Scand 1985;56:25–27.

Elves MW, Bayley I, Roylance PJ. The effect of indomethacin upon experimental fractures in the rat. Acta Orthop Scand 1982;53:35–41.

Engsig MT, Chen QJ, Vu TH, Pedersen AC, Therkidsen B, Lund LR, Henriksen K, Lenhard T, Foged NT, Werb Z, Delaisse JM. Matrix metalloproteinase 9 and vascular endothelial growth factor are essential for osteoclast recruitment into developing long bones. J Cell Biol 2000;151:879–889.

Forwood MR. Inducible cyclo-oxygenase (COX-2) mediates the induction of bone formation by mechanical loading in vivo. J Bone Miner Res 1996;11:1688–1693.

Fujioka H, Tsunoda M, Noda M, Matsui N, Mizuno K. Treatment of ununited fracture of the hook of hamate by low-intensity pulsed ultrasound: A case report. J Hand Surg [Am] 2000;25:77–79.

Gallo O, Franchi A, Magnelli L, Sardi I, Vannacci A, Boddi V, Chiarugi V, Masini E. Cyclooxygenase-2 pathway correlates with VEGF expression in head and neck cancer. Implications for tumor angiogenesis and metastasis. Neoplasia 2001;3:53–61.

Gerber HP, Vu TH, Ryan AM, Kowalski J, Werb Z, Ferrara N. VEGF couples hypertrophic cartilage remodeling, ossification and angiogenesis during endochondral bone formation. Nat Med 1999;5:623–628.

Kawaguchi H, Raisz LG, Voznesensky OS, Alander CB, Hakeda Y, Pilbeam CC. Regulation of the two prostaglandin G/H synthases by parathyroid hormone, interleukin-1, cortisol, and prostaglandin E2 in cultured neonatal mouse calvariae. Endocrinology 1994;135:1157–1164.

Kawata A, Mikuni-Takagaki Y. Mechanotransduction in stretched osteocytes—Temporal expression of immediate early and other genes. Biochem Biophys Res Commun 1998;246:404–408.

Keller J, Klamer A, Bak B, Suder P. Effect of local prostaglandin E2 on fracture callus in rabbits. Acta Orthop Scand 1993;64:59–63.

Meyer RA, Meyer MH, Phieffer LS, Banks DM. Delayed union of femoral fractures in older rats:decreased gene expression. BMC Musculoskelet Disord 2001;2:2.

Naik AA, Xie C, Zuscik MJ, Kingsley P, Schwarz EM, Awad H, Guldberg R, Drissi H, Puzas JE, Boyce B, Zhang X, O'Keefe RJ. Reduced COX-2 expression in aged mice is associated with impaired fracture healing. J Bone Miner Res 2009;24:251–264.

Nakajima F, Ogasawara A, Goto K, Moriya H, Ninomiya Y, Einhorn TA, Yamazaki M. Spatial and temporal gene expression in chondrogenesis during fracture healing and the effects of basic fibroblast growth factor. J Orthop Res 2001;19:935–944.

Naruse K, Mikuni-Takagaki Y, Azuma Y, Ito M, Oota T, Kameyama K, Itoman M. Anabolic response of mouse bone-marrow-derived stromal cell clone ST2 cells to low-intensity pulsed ultrasound. Biochem Biophys Res Commun 2000;268:216–220.

Naruse K, Miyauchi A, Itoman M, Mikuni-Takagaki Y. Distinct anabolic response of osteoblast to low-intensity pulsed ultrasound. J Bone Miner Res 2003;18:360–369.

Nelson FR, Brighton CT, Ryaby J, Simon BJ, Nielson JH, Lorich DG, Bolander M, Seelig J. Use of physical forces in bone healing. J Am Acad Orthop Surg 2003;11:344–354.

Nilsson BE, Edwards P. Age and fracture healing: a statistical analysis of 418 cases of tibial shaft fractures. Geriatrics 1969;24:112–117.

Peng H, Wright V, Usas A, Gearhart B, Shen HC, Cummins J, Huard J. Synergistic enhancement of bone formation and healing by stem cell-expressed VEGF and bone morphogenetic protein-4. J Clin Invest 2002;110:751–759.

Rawool NM, Goldberg BB, Forsberg F, Winder AA, Hume E. Power Doppler assessment of vascular changes during fracture treatment with low-intensity ultrasound. J Ultrasound Med 2003;22:145–153.

Reuter U, Strempel F, John F, Knoch HG. [Modification of bone fracture healing by ultrasound in an animal experiment model]. Z Exp Chir Transplant Kunstliche Organe 1984;17:290–297.

Ruegsegger P, Koller B, Muller R. A microtomographic system for the nondestructive evaluation of bone architecture. Calcif Tissue Int 1996;58:24–29.

Rundle CH, Strong DD, Chen ST, Linkhart TA, Sheng MH, Wergedal JE, Lau KH, Baylink DJ. Retroviral-based gene therapy with cyclooxygenase-2 promotes the union of bony callus tissues and accelerates fracture healing in the rat. J Gene Med 2008;10: 229–241.

Street J, Bao M, deGuzman L, Bunting S, Peale FV Jr, Ferrara N, Steinmetz H, Hoeffel J, Cleland JL, Daugherty A, van Bruggen N, Redmond HP, Carano RA, Filvaroff EH. Vascular endothelial growth factor stimulates bone repair by promoting angiogenesis and bone turnover. Proc Natl Acad Sci U S A 2002;99:9656–9661.

Street JT, Wang JH, Wu QD, Wakai A, McGuinness A, Redmond HP. The angiogenic response to skeletal injury is preserved in the elderly. J Orthop Res 2001;19:1057–1066.

Sudmann E, Hagen T. Indomethacin-induced delayed fracture healing. Arch Orthop Unfallchir 1976;85:151–154.

Tsukii K, Shima N, Mochizuki S, Yamaguchi K, Kinosaki M, Yano K, Shibata O, Udagawa N, Yasuda H, Suda T, Higashio K. Osteoclast differentiation factor mediates an essential signal for bone resorption induced by 1 alpha,25-dihydroxyvitamin D3, prostaglandin E2, or parathyroid hormone in the microenvironment of bone. Biochem Biophys Res Commun 1998;246:337–341.

Yang KH, Parvizi J, Wang SJ, Lewallen DG, Kinnick RR, Greenleaf JF, Bolander ME. Exposure to low-intensity ultrasound increases aggrecan gene expression in a rat femur fracture model. J Orthop Res 1996; 14:802–809.

Cell Tissue Bank
DOI 10.1007/s10561-010-9185-5

ORIGINAL PAPER

A new technique for seeding chondrocytes onto solvent-preserved human meniscus using the chemokinetic effect of recombinant human bone morphogenetic protein-2

Hiroaki Minehara · Ken Urabe · Kouji Naruse · Alexander T. Mehlhorn · Kentaroo Uchida · Norbert P. Südkamp · Moritoshi Itoman

Received: 16 December 2009 / Accepted: 28 May 2010

Abstract Many investigators are currently studying the use of decellularized tissue allografts from human cadavers as scaffolds onto which patients' cells could be seeded, or as carriers for genetically engineered cells to aid cell transplantation. However, it is difficult to seed cells onto very dense regular connective tissue which has few interstitial spaces. Here, we discuss the development of a chemotactic cell seeding technique using solvent-preserved human meniscus. A chemokinetic response to recombinant human bone morphogenetic protein-2 (rhBMP-2) was observed in a monolayer culture of primary chondrocytes derived from femoral epiphyseal cartilage of 2-day-old rats. The rhBMP-2 significantly increased their migration upto 10 ng/ml in a dose-dependent manner. When tested with solvent-preserved human meniscus as a scaffold, which has few interstitial spaces, rhBMP-2 was able to induce chondrocytes to migrate into the meniscus. After a 3-week incubation, newly-formed cartilaginous extracellular matrix was synthesized by migrated chondrocytes throughout the meniscus, down to a depth of 3 mm. These findings demonstrate that rhBMP-2 may be a natural chemokinetic factor in vivo, which induces migration of proliferative chondrocytes into the narrow interfibrous spaces. Our results suggest a potential application of rhBMP-2 for the designed distribution of chondrocytes into a scaffold to be used for tissue engineering.

Keywords BMP-2 · Chondrocytes · Cell migration · Chemokinesis

H. Minehara · K. Urabe (✉) · K. Naruse · K. Uchida · M. Itoman
Department of Orthopaedic Surgery, Kitasato University School of Medicine, 1-15-1 Kitasato, Sagamihara, Japan
e-mail: kenurabe@med.kitasato-u.ac.jp

A. T. Mehlhorn · N. P. Südkamp
Department of Orthopaedic and Trauma Surgery, Albert-Ludwig University, Freiburg, Germany

Published online: 17 June 2010

Introduction

In most tissue engineering approaches, cells are typically isolated from a small biopsy sample and then expanded in culture. These expanded cells are then seeded onto a suitable three-dimensional scaffold and induced to produce a tissue-like structure in vitro. The composites of cells and scaffold are then implanted in vivo into an orthotopic site to repair damaged tissue. The phenotype of a cell-based tissue-engineered construct depends on a number of factors, such as the composition, size, porosity and biodegradability of the scaffold, as well as the cell type, cell density, and spatial distribution of the cells within the construct (Langer 2000). The cellularity of the engineered construct depends on the number of cells initially introduced into the construct, on the retention of these cells during the first few hours to days until cell-cell and cell-scaffold interactions have

been established, and on the mitotic activity of the cells incorporated into the construct (Solchaga et al. 2006). For any given scaffold, the initial seeding influences cell density, retention, and spatial distribution within the scaffold, all of which will eventually affect the function of the construct (Griffon et al. 2005; Holy et al. 2000; Mauck et al. 2002) .

Currently, there are a variety of methods used for seeding cells into a three-dimensional matrix with the aim of achieving uniform cell distribution (Griffon et al. 2005; Solchaga et al. 2006; Thevenot et al. 2008; Timmins et al. 2007; Wendt et al. 2003). In the passive methods of seeding, cells are laid on top of the scaffold and allowed to infiltrate into the scaffold over time (Wendt et al. 2003). The main disadvantage, particularly in the case of thick scaffolds with high degrees of tortuosity, is that the infiltration rates can be very low, resulting in poor loading and uneven distribution of cells within the scaffolds. In the active methods of seeding, an external force is applied to encourage the cells to infiltrate into the porous scaffold (Cimetta et al. 2007; Griffon et al. 2005; Mauck et al. 2002). The nature of the force varies from centrifugal to external pressure gradients, vacuum and compression force (Griffon et al. 2005; Griffon et al. 2005; Thevenot et al. 2008). However, it is difficult to seed cells into high density regular connective tissue which has few interstitial spaces. Here, we discuss the development of a chemotactic cell seeding technique using solvent-preserved human meniscus which has a highly dense collagen structure.

Bone morphogenetic protein (BMP)-2, a member of the transforming growth factor (TGF)-β superfamily (Chen et al. 1991a, b; Massague 1992; Sampath et al. 1990; Wozney et al. 1988) plays an important role in the differentiation of mesenchymal cells. Generally, BMP-2 stimulates cell differentiation when the concentration is higher than 100–500 ng/ml in vitro (Date et al. 2004; Kawasaki et al. 1998; Ryoo et al. 2006; Sekiya et al. 2005). On the other hand, BMP-2 also affects migration of mesenchymal cells, fibroblasts and osteoblasts (Bhardwaj et al. 2001; Fiedler et al. 2002; Lind et al. 1996; Uchida et al. 2007) but the concentration of BMP-2 required for cell migration is lower than that for differentiation. Migratory effects of BMP-2 have also been noted in endothelial cells or smooth muscle cells, but rarely in chondrocytes.

Bhargava et al. (1999) have evaluated the migratory effects of several cytokines including BMP-2 on bovine meniscus cells. The meniscus-derived cells, which may contain chondrocytic cells, were not well characterized in the study. Isolated chondrocytes are easy to irreversibly dedifferentiate in monolayer culture (Mukaida et al. 2005) and therefore, it is unclear whether the cells used by Bhargava et al. (1999) still retained the biological characteristics of meniscus chondrocytes. In addition to the reported effect of BMP-2 on chondrocyte differentiation and cartilage matrix formation (Erickson et al. 1997; Stewart et al. 2004), we considered that investigation of the chemotactic and/or chemokinetic effect of BMP-2 on chondrocytes would be necessary. We also hypothesized that the migratory effect of BMP-2 on chondrocytes could be useful for chondrocyte seeding into solvent-preserved human meniscus.

In this study we used proliferating chondrocytes isolated from the distal epiphysis of 2 day old Wistar rats and evaluated the response of chondrocytes to BMP-2. We also developed a chondrocyte seeding technique into solvent-preserved human meniscus using the migratory response of chondrocytes to BMP-2.

Materials and methods

Preparation of proliferating chondrocytes

All the procedures involving animals were carried out in accordance with the guidelines of Kitasato University Animal Ethics Committee. Chondrocytes in the distal epiphysis were harvested from 2 day old Wistar rat femora. The distal femora were exposed and adherent soft tissues were stripped. The reserved zone of the epiphysis was removed by dissection. The cartilage fragments containing the reserved zone chondrocytes were washed three times in PBS (Wako) containing antibiotics (streptomycin, penicillin, fungizone (GIBCO-Invitrogen, Carlsbad, CA)) and digested for 4 h in a 0.3% solution of Collagenase P (GIBCO) in PBS in a shaking water bath at 37°C. The solution containing the isolated cells was filtered through 70-μ mesh and the cells recovered by centrifugation at 1,000 rpm at 4°C and resuspended in Ham's F-12 medium (Biochrom AG, Berlin, Germany) containing antibiotics and 10% FBS at a

final concentration of 2×10^5 cells/ml. The isolated cells were used for each experiment immediately after isolation.

Migratory response of chondrocytes to rhBMP-2

Disposable 96-well chemotaxis chambers (Neuro Probe, Gaithersburg, MD) were used (Albini et al. 1987; Uchida et al. 2007). Recombinant hBMP-2 (R & D systems, Minneapolis, MN) was added to a final concentration of 0.01, 0.1, 1, 10 or 100 ng/ml in Dulbecco's modified Eagle's medium (DMEM; Cambrex, Walkersville, MD) containing 1 % antibiotic mixture (GIBCO). Primary proliferating chondrocytes (1×10^4 cells/well) were seeded in Ham's F-12 medium onto the membrane of the chamber set in a 6-well plate. Cell number was standardized using a curve prepared from 0, 25, 50, 100, 200, 400, 800 and 1,600 cells/50 µl solution. The chemotaxis chamber was incubated in 5% CO_2 at 37°C for 48 h. Cells were then labelled with 2.5 µM Calcein acetoxymethyl ester (AM) after eliminating the non-migrant cells (Uchida et al. 2007) and the fluorescence of each sample was measured by a plate reader (Spectra Fluor Plus, Tecan, Finland).

The chemotactic responses of chondrocytes were tested by checkerboard analysis to determine whether cell migration was due to chemotaxis (i.e., cell migration in response to a concentration gradient) or chemokinesis (i.e., cell migration irrespective of a concentration gradient) (Fiedler et al. 2002). Four culture conditions were prepared, as follows. Equal concentration gradient: culture medium in both top and bottom wells of a Boyden chamber contained 100 ng/ml rhBMP-2; positive concentration gradient: only the medium in the bottom well contained 100 ng/ml rhBMP-2; negative concentration gradient: only the medium in the top well contained BMP-2. Absent concentration gradient was the condition in which neither the medium in the top nor the bottom contained 100 ng/ml rhBMP-2.

Scratch assay

We assessed the chemokinetic effect of rhBMP-2 using the scratch assay. Rat primary proliferating chondrocytes (2×10^4 cells/well) were seeded into a 6-well plate when the cells reached sub-confluence. After culturing in DMEM containing 10% foetal bovine serum (FBS; Sigma, Japan) and antibiotics for 8 h, medium was replaced with the same medium without FBS, then a scratch was gently made with a sterile 200 µl pipette tip across the centre of the plate. After two washes with serum free DMEM, the cells were incubated in the same medium in the presence or absence of 10 ng/ml rhBMP-2. Cell migration into the scratched area was photographed at 0, 12, 24, 36 and 48 h and the cell number was counted using NIH image software (NIH, Bethesda, MD) (Katsumoto et al. 2005; Nishio et al. 2005; Zhang et al. 2004).

Preparation of preserved menisci

Preserved menisci were provided by Tutogen Medical Inc. (Neunkirchen, Germany). Menisci were retrieved from cadaveric donors who gave informed consent for cadaveric donations. Donors did not receive any monetary compensation. Donor suitability was established by the medical director in accordance with American Association of Tissue Banks (AATB) standards and Food and Drug Administration (FDA) regulations. Prior to retrieval, a physical examination, medical, social and sexual history inquiry, medical history and medical records review were performed to screen for infections, adverse conditions, risk factors and malignancies. The autopsy report was also checked. Serological tests for infectious diseases were performed.

The retrieved menisci were processed through delipidation, osmotic treatment, oxidation, dehydration and irradiation. Tissue underwent an acetone bath to remove the fat tissues, and the graft was washed in alternating baths of distilled water and saline for osmotic contrast treatment to remove cellular materials. The graft was bathed in hydrogen peroxide washes for oxidative treatment to destroy proteins and immunogenic structures. The graft was then passed through a series of acetone baths for solvent dehydration and viral inactivation to prohibit the growth of microbes and inactivate viruses. Following product packing, the graft was subjected to low-dose gamma irradiation (17–20 kGy). The process required only validated minimal doses of irradiation, thereby preserving the biomechanical integrity of the graft while ensuring post-packaging sterility.

Evaluation of migrated chondrocytes within the dense tissues

Supplied menisci with an average pore size of 10 μm were punched out perpendicularly to the surface (see Fig. 3 for a representative meniscus) to form a small column. The same culture medium as that used in the scratch test was prepared. Fifty microliters of medium with or without 10 ng/ml rhBMP-2 was added to the micro-tube. Each piece of meniscus was plugged tightly into a micro-tube so that the bottom of the meniscus was soaked in the solution. Chondrocytes (2×10^4) were then placed on top of the column and cultured for 24 h in 5% CO_2 at 37°C. Following this 24-h incubation, the meniscus columns were washed 3 times with medium to remove rhBMP-2 and non-adherent cells. The cells which had penetrated into the columns were then cultured in DMEM with 10% FBS and antibiotics for 3 weeks. Paraffin sections were prepared for Hematoxylin-Eosin and Safranin-O staining for histological observation.

Statistical analysis

One-way ANOVA with Tukey's multiple comparison test was used. All tests were two-tailed, with differences considered significant * at $P < 0.05$.

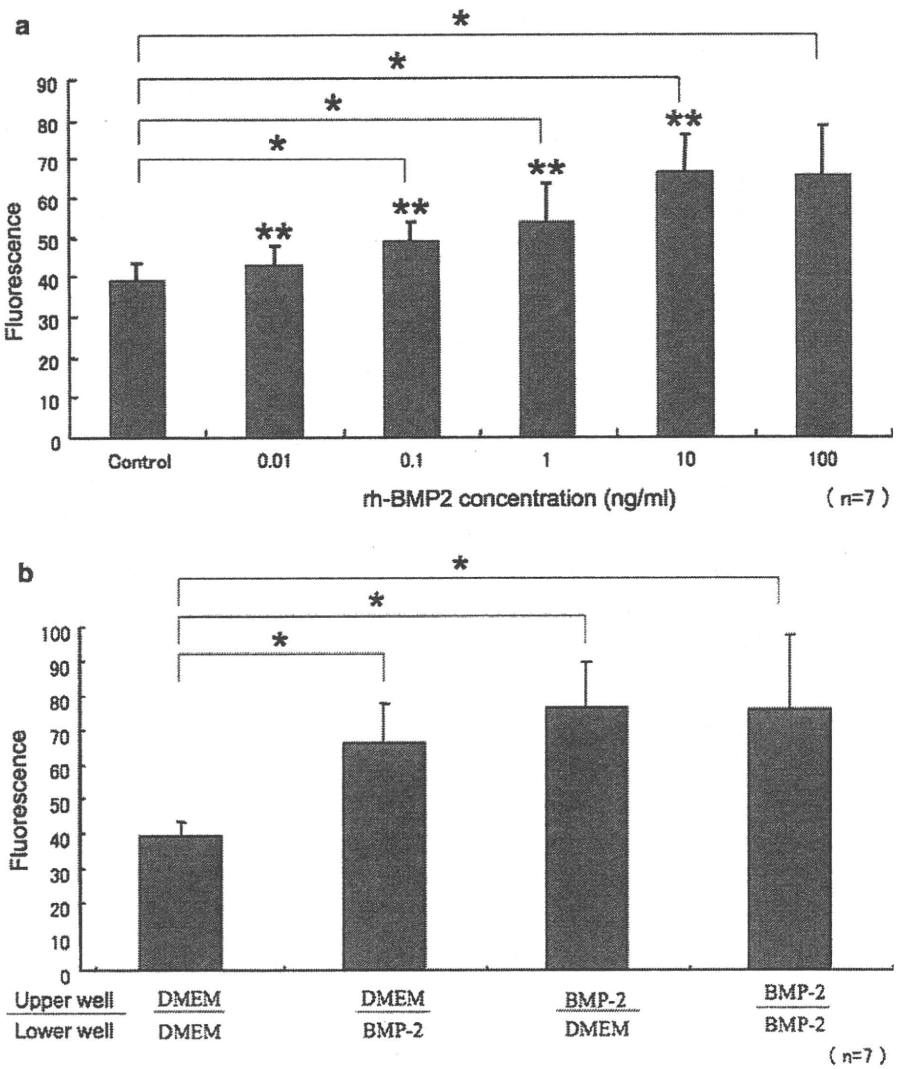

Fig. 1 Migratory effect of recombinant human BMP-2 (rhBMP2) on chondrocytes. **a** Chemotaxis chamber analysis. Increasing concentrations of rhBMP-2 from 0.01 to 10 ng/ml increased the intensity of fluorescence. However the levels of intensity between 10 and 100 ng/ml were similar. **b** Checkerboard analysis. This analysis showed that the migratory effect of rhBMP-2 on chondrocytes was due to chemokinesis

Results

Migratory response of epiphyseal proliferating chondrocytes to rhBMP-2

The basal numbers of migrated cells in the chemotaxis chambers were in proportion to the numbers of seeded cells (data not shown). The number of migrated cells increased with the addition of rhBMP-2 in a dose dependent manner between 0.01 and 10 ng/ml (Fig. 1a), and then levelled off above 10 ng/ml. The increments showed a significant difference compared to the control value as depicted in Fig. 1. The numbers of migrated cells in positive, negative and equal concentration gradients were significantly higher than that in the absent concentration gradient, and there

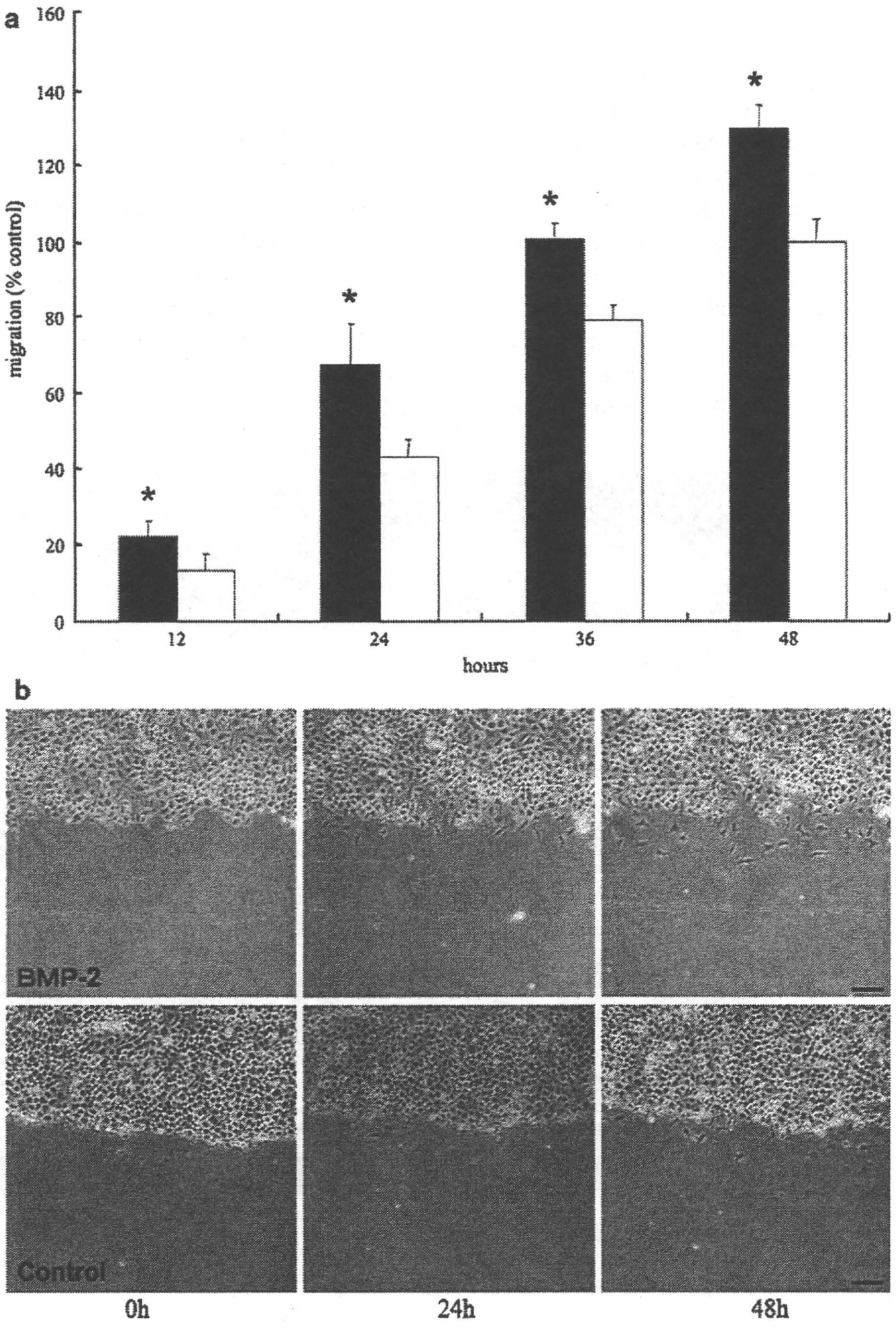

Fig. 2 Scratch assay. **a** Percentage of cell migration. Each value was calculated as the percentage of the area covered at each time point divided by the area covered at 48 h in control. *Black* and *white* bars symbolize the percentages of the recombinant human BMP-2 (rhBMP-2) group and control, respectively. A significantly higher migration rate in proportion to time was observed in the rhBMP-2 group when compared to control. **b** The appearance of the scratched area. The number of migrated cells in the scratched area of a 6-well plate was increased in the rhBMPf-2 group when compared to control. *Scale bars* represent 100 μm

were no differences between positive, negative and equal concentration gradients (Fig. 1b). The scratch assay showed a significantly higher rate of migration in the rhBMP-2 group at all time points measured (Fig. 2a, b). These results indicate that the effect of rhBMP-2 on chondrocyte migration is not chemotactic but chemokinetic.

Chondrocyte migration into the dense meniscus tissue

Scanning electron microscopy showed that the diameter of the interstitial spaces within the preserved human menisci used for this study was approximately 10–20 μm with the fibrous tissue structure maintained (data not shown). H.E. stained sections of preserved meniscal tissue suggested the homogeneous orientation of collagen fibres and interstitial spaces (Fig. 3b). Both cells and extracellular matrix could be recognized in the meniscus columns cultured for 3 weeks after 24-h rhBMP-2 treatment, but not in the columns cultured without BMP treatment (Fig. 4). In the H.E. stained sections, newly synthesized extracellular matrix was observed between the existing fibrous components (Fig. 4a). This area stained red with Safranin-O (Fig. 4c). The cells and matrix were distributed homogeneously from the tissue surface to the bottom of the column (data not shown). The fibrous structure of the meniscus was either distorted or apparently degraded by the newly formed extracellular matrix (Fig. 4a, c). No cells or newly synthesized extracellular matrix were seen in the control cultures not treated with rhBMP-2 (Fig. 4b, d).

Discussion

In dense regular connective tissues such as tendons and ligaments, parallel arrays of fibrils and fascicles are uniaxially aligned into cable-like fibrillar structures that maintain the mechanical integrity and strength necessary for their load-bearing function. Many investigators are currently studying the use of decellularized tissue allografts from human cadavers

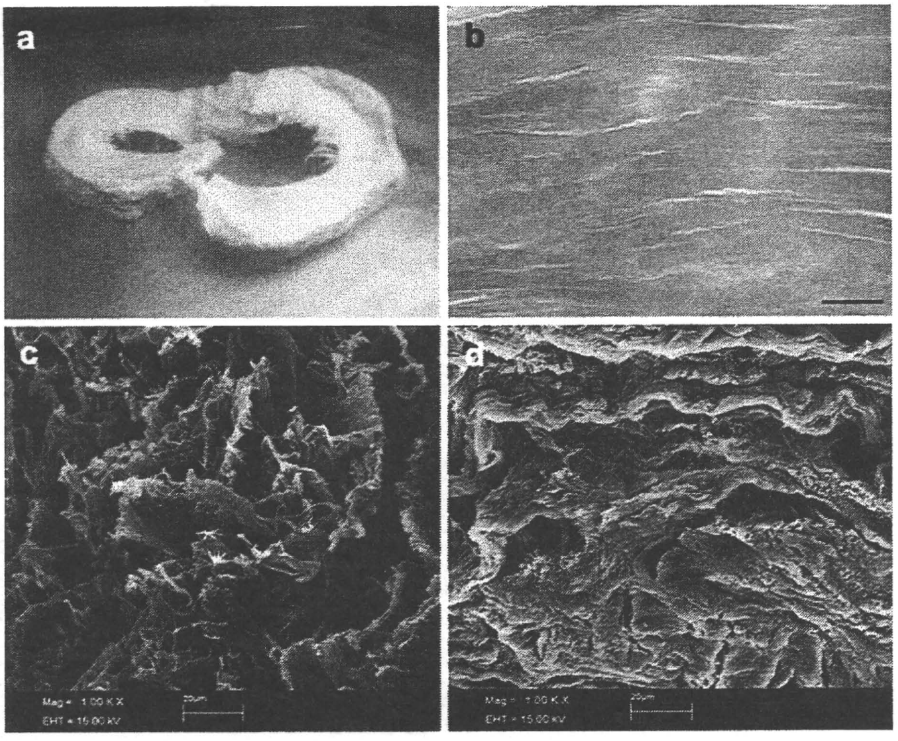

Fig. 3 Evaluation of solvent preserved meniscus from human cadavers. **a** Gross appearance of solvent preserved meniscus. The meniscus was punched out perpendicularly to the surface to form a small column. **b** H.E. stained section of preserved meniscus. No cells were evident and collagen fibers were homogeneously stained with eosin. *Scale bars* represent 100 μm